Manuscript prepared for Biogeosciences
with version 2014/09/16 7.15 Copernicus papers of the LaTeX class copernicus.cls.
Date: 6 April 2015

Peru Upwelling Plankton Respiration: Calculations of Carbon Flux, Nutrient Retention Efficiency and Heterotrophic Energy Production

T.T. Packard[1], N. Osma[1], I. Fernández-Urruzola[1], L. A. Codispoti[2], J. P. Christensen[3], and M. Gómez[1]

[1]Marine Ecophysiology Group (EOMAR), Universidad de Las Palmas de Gran Canaria, Campus Universitario de Tafira 35017, Spain
[2]Horn Point Laboratory, University of Maryland, 21613-0775 Cambridge Maryland, USA
[3]Green Eyes LLC, Easton, MD. 21601, USA

Correspondence to: T.T. Packard (theodoretrainpackard@gmail.com)

Abstract. Oceanic depth profiles of plankton respiration are described by a power function, R_{CO_2} = $(R_{CO_2})_0$ $(z/z_0)^b$ similar to the vertical carbon flux profile. Furthermore, because both ocean processes are closely related, conceptually and mathematically, each can be calculated from the other. The exponent, b, always negative, defines the maximum curvature of the respiration depth-profile and controls the carbon flux. When |b| is large, the carbon-flux (F_C) from the epipelagic ocean is low and the nutrient retention efficiency (NRE) are high allowing these waters to maintain high productivity. The opposite occurs when |b| is small. This means that the attenuation of respiration in ocean water columns is critical in understanding and predicting both vertical F_C as well as the capacity of epipelagic ecosystems to retain their nutrients. The ratio of seawater R_{CO_2} to incoming F_C is the NRE, a new metric that represents nutrient regeneration in a seawater layer in reference to the nutrients introduced into that layer via F_C. A depth-profile of F_C is the integral of water column respiration. This relationship facilitates calculating ocean sections of F_C from water column respiration. In a F_C section and in a NRE section across the Peru upwelling system we found a F_C and an NRE minimum extending down to 400 m, 50 km off the Peru coast over the upper part of the continental slope. Finally, coupling respiratory electron transport system activity to heterotrophic oxidative phosphorylation promoted the calculation of an ocean section of heterotrophic energy production (HEP). It ranged from 250 to 500 J d^{-1} m^{-3} in the euphotic zone, to less than 5 J d^{-1} m^{-3} below 200 m on this ocean section.

1 Introduction

Respiration is as ubiquitous in the ocean as are the microorganisms that cause it (Seiwell, 1934; Richards, 1957; Lane, 2002). It is controlled by the respiratory electron transport (ETS) activity in eukaryotic mitochondria and prokaryotic cell membranes (Packard, 1969; Packard et al., 1971; Lane, 2005; Nelson and Cox., 2000) and is responsible for the bulk of oceanic O_2 consumption (Seiwell, 1937; Redfield et al., 1963; Packard, 1985a). It is driven by the degradation of dissolved and particulate organic carbon, generates CO_2 (Redfield et al., 1963), acidifies seawater (Harvey, 1955), and produces energy in the form of ATP (heterotrophic energy production) (Ochoa, 1943; Nelson and Cox., 2000; Madigan et al., 2000). Even in anoxic seawater respiration degrades organic matter, produces CO_2, and generates ATP while reducing nitrogen oxides to N_2 or SO_4^- to H_2S (Richards, 1965; Madigan et al., 2000). Plankton community respiration in the ocean's water column is a key variable in calculating net community productivity (Ducklow and Doney, 2013) in developing oceanic carbon models, in resolving the autotrophic-heterotrophic states of ocean ecosystems (Williams et al., 2012), and in understanding vertical ocean F_C rates (Giering et al., 2014). The research team led by Sarah Giering (Giering et al., 2014) demonstrated that, contrary to previous efforts (Burd et al., 2010), but in accord with classical oceanographic understanding (Riley, 1951; Richards, 1957; Redfield et al., 1963; Suess, 1980), zooplankton and microplankton (prokaryote and eukaryote) respiration balance vertical carbon flux (Riley, 1951; Eppley and Peterson, 1979; Packard et al., 1988). All these findings support the use of plankton respiration in assessing vertical F_C in the ocean water column. Conceptually, the reciprocal relationship of the water column respiration and the F_C, from the ocean's epipelagic zone, is clear (Suess, 1980; Martin et al., 1987). However, describing this reciprocal relationship mathematically, as a function of ocean depth in the forms,

$$R = f(z) \ and \ F_C = \int_{z_1}^{z_2} R dz$$

was delayed until the helium-tritium studies of Jenkins (Jenkins, 1982, 1984), the sediment trap studies of VERTEX program (Martin et al., 1987), and respiratory electron transport system (ETS) measurements in the Gulf of Maine (Packard and Christensen, 2004). In the later, microplankton ETS measurements were used to build power function models of respiratory CO_2 production (R_{CO_2}) and F_C. Here, we extend this approach to calculate a microplankton respiration section across the Peru Upwelling System ((Walsh, 1972; Barber et al., 1971) and Fig. 1a) and to model F_C on this transect. We focused our measurements on microplankton because its biomass and metabolism dominate ocean water columns (King et al., 1978; Arístegui et al., 2009; Laufkötter et al., 2013). The section was made at a time of regime-change when the Peru upwelling system and the El Niño-Southern Oscillation (ENSO) underwent a shift (Santoso et al., 2013). Here we document some of the biological phenomenon that occurred at that time. With the F_C and the R_{CO_2} models we calculate the nutrient retention efficiency (Packard and Gómez, 2013; Osma et al., 2014), a new metric that quan-

tifies the ability of an ocean layer to retain its nutrients (Fig. 2c). Conceptually, the nutrient retention efficiency (NRE) is the nutrient remineralization rate within an ocean layer normalized by nutrients entering that layer via carbon-flux. Below the euphotic zone it can be calculated as the inverse of the F_C transfer efficiency (Buesseler et al., 2007; Buesseler and Boyd, 2009), but we show here that it can also be calculated from a profile of plankton respiration. In addition, using different limits to the F_C integration we calculate the sum of the benthic respiration and carbon burial (Fig. 3a) that occurs on the sea floor. Finally we use the respiration models and the couple between ETS activity and oxidative phosphorylation to calculate light-independent heterotrophic energy flow (Karl, 2014). This energy is generated in the form of ATP by ATP synthase, an enzyme motor coupled to a heterotrophic respiratory process such as O_2 utilization or NO_3^- reduction (Watt et al., 2010; Ferguson, 2010). In all types of respiration, the ATP synthase senses the pH and electromotive force gradient across the membrane in which the ATP synthase is embedded (Lane et al., 2010) and when the gradient is sufficiently strong ($\sim$ 225 mV), the molecular motor that is the ATP synthase, starts its rotary production of ATP (Walker, 1998). Heterotrophic ATP generation in any ecosystem is largely based on exploiting the Gibbs Free Energy (ΔG) released during the oxidation of different organic compounds. The biochemistry of ATP and the ETS was unknown in 1925, but even then the idea of capturing biologically useable energy from respiration was appreciated by Lotka (1925). A generation later Odum built on this concept to describe energy flow in fresh water streams (Odum, 1956). Reviewing this earlier work, Karl recently argued that biological energy production in the ocean should be assessed to provide insight to variability in ocean productivity (Karl, 2014). Here, we address his concern by calculating Heterotrophic Energy Production (HEP) in a C-Line section (Fig. 2d). This HEP is the energy produced while ATP is generated by respiratory O_2 consumption (R_{O_2}) in the microplankton community composed of phytoplankton, bacteria, archea, and protozoans in the epipelagic layer and by the R_{O_2} and NO_3^- reduction in microbial communities of bacteria, archea, and protozoans in the meso- and bathypelagic waters of the Peru Current upwelling system.

2 Methods

2.1 Research site

The site of this CUEA investigation at 15°S off Pisco Peru (Fig. 1) was chosen because the upwelling is strong, persistent, and well known (Wooster, 1961; Fernández et al., 2009). It was the focus of the R/V Anton Bruun cruise 15 (Ryther et al., 1970), the R/V T.G. Thompson Pisco expedition in 1969 (Barber et al., 1978), and others (Wyrtki, 1967; Walsh et al., 1971) before it was the focus of the CUEA-JOINT II program (Brink et al., 1981; Packard, 1981) of which the JASON Expedition was a part (King, 1981; Richards, 1981). However, in spite of the many previous expeditions to this site most of them took place in the austral fall (March-April-May). The JASON-76 expedition was unique because it took place in the late winter and austral spring (August, September, October, and

November) when the southeast trade winds would be at their strongest (Wooster, 1961). In this way it was thought that the results might be more comparable with results from upwelling studies made in the northern hemisphere's spring-time upwelling off NW Africa (Codispoti et al., 1982; Minas et al., 1982). The results presented here are from the September 10 to September 24 leg of JASON-76 on board Duke University's Oceanographic ship, R/V Eastward, cruise number, E-5H-67 (Packard and Jones, 1976).

2.2 Sampling

All sampling was conducted along the C-Line (Fig. 1a) that extended seaward from the coast at position C1, just south of Cabo Nazca (Pisco), across the deep trench to position C14, 185 km offshore (Packard, 1981). Hydrographic sections were made at the beginning of the expedition (10-11 September) and again after a lapse of 10 days (20-21 September). The endpoint coordinates were from 15°3.2'S, 75°26.0'W to 15°55.8'S, 75°31.4'W (Packard and Jones, 1976; Kogelshatz et al., 1978). In addition, between 10 and 24 September, productivity stations, that focused on the biological, nutrient chemistry, and biochemical properties at depths where the light was 100, 50, 30, 15, 5, 1, and 0.1% of the surface incident radiation (light-depths), were made at C-Line positions Packard and Jones (1976). These productivity stations were not made in order along the C-line section, hence the irregularity of the their numerical sequence in Tables 3-7. In addition, some locations along the C-Line were occupied several times. For this reason, as well as to coordinate the results presented here with the results of other CUEA reports (Brink et al., 1981), both the C-Line location and the station number are given through the paper. The productivity casts were made each morning before 10:00 with 30 L Niskin PVC bottles to 6 light-depths (1, 5, 15, 30, 50, and 100%). Each Niskin bottle was flushed at depth in yo-yo fashion both by the action of the ship's roll and by meter oscillations with the winch. On deck it was drained immediately, without prefiltration, into a well rinsed carboy for subsampling and returned to depth for the next sample. The six samples were taken within an hour. Subsamples were drawn for phytoplankton productivity, inorganic nutrient salts, (ammonium, reactive phosphorus, NO_3^-, NO_2^- and silicate), ETS and NO_3^- reductase activities, and particulate protein (Packard and Jones, 1976). Station coordinates are given in Table 1. The inorganic nutrient salts, salinity, temperature, and O_2 can be found in CUEA data reports 38 and 45 (Hafferty et al., 1978; Kogelshatz et al., 1978). Chlorophyll, and phytoplankton productivity (^{14}C-uptake) are reported in CUEA data report (Barber et al., 1978). The ^{14}Carbon-uptake data were calculated on an hourly basis (Table 1) from the 24 h-productivity data (Kogelshatz et al., 1978). Light was measured as daily total solar radiation with an Eppley Model 8-48 pyranometer placed above the ship's bridge (Packard and Jones, 1976). Below the mesopelagic zone the seawater was sampled for ETS activity with 30L Niskin PVC bottles down to 2000m, depending on the depth of the water column (Tables 2 and 3).

2.3 ETS activity, respiratory O_2 consumption, CO_2 production, and denitrification

Respiratory ETS activity in the euphoric zone (Ez) was measured according to Kenner and Ahmed (1975) as described in Packard and Williams (1981). In deeper waters it was measured according to (Packard et al., 1971) and multiplied by 3.35 to render the two data sets comparable as explained in Christensen and Packard (1979). Here, ETS activity is used as a direct measure of potential respiration and a proxy for respiration. Both potential respiration and respiration were calculated from the combined ETS data set according to Packard and Christensen (2004) and Packard and Codispoti (2007). Tables 2 and 3 explain the calculations in detail. Table 3 presents the calculations as R_{O_2} in units of μmol O_2 m^{-3} h^{-1} for oxic waters. Using ETS activity as a proxy for R_{O_2} requires selection of a ratio of potential respiration (Φ) to R_{O_2}. Since direct measurements of R_{O_2} can not be made below the euphoric zone, a true calibration can not be made. The Φ to R_{O_2} ratio should range around 0.5 if Φ represents V_{max} of the ETS and standard physiological rates, governed by enzyme activities, operate close to 1/2 their potential capacity (Cleland, 1967). In our hands (sense Schatteman et al. (1988); Sigman et al. (1997)), with our methodology (Packard and Williams, 1981), and by our analysis (Packard and Christensen, 2004) we calculated a Φ to R_{O_2} ratio, 0.26 (Table 2), that successfully predicted R_{O_2} in the epipelagic and the mesopelagic waters of the Nansen Basin of the Arctic Ocean (Packard and Codispoti, 2007). In that study, R_{O_2} was a long-term average R_{O_2} calculated by the AOU-He-tritium method of Jenkins (1982, 1984) as used by W. Roether in Zheng et al. (1997). We have chosen to use the same Φ-to-R_{O_2} ratio of 0.26 here (Table 2 and 3). R_{CO_2} (Fig. 2a) was then calculated from R_{O_2} using a Redfield ratio (C/O_2) of 0.71 from Takahashi et al. (1985). This is the best available way to calculate water respiration from our water column ETS measurements.

In waters where respiration is based on using oxides of nitrogen (NO_3^-, NO_2^-, N_2O, or NO) in place of O_2, calculations are different. Since microbial respiratory NO_3^- reduction to nitrogen gas (denitrification) occurs in the water column between 47 and 400 m between positions C3 to C12 (Garfield et al., 1979; Codispoti and Packard, 1980) (Fig. 2a), Table 3 presents denitrification rates from these depths (shaded numbers) as R_{N_2} in units of μmol N_2 m^{-3} h^{-1}. In these oxygen-defficient waters we used a Redfield ratio, C/N_2, from Gruber and Sarmiento (1997). To apply it, one first has to calculate R_{N_2} based on the fact that the ETS for R_{O_2} and R_{N_2} differ only in the terminal electron acceptor (Packard, 1969; Chen and Strous, 2013). This was done in Tables 2 and 3 according to Codispoti and Packard (1980) and Codispoti et al. (2001). The approach has recently been corroborated by Dalsgaard et al. (2012). R_{N_2} in units of micromole N_2 $h^{-1}1$ m^{-3} is calculated in Table 2, column 2, by multiplying nanoeq min^{-1} L^{-1} by 60. The product is equivalent to micro mol e^- h^{-1} m^{-3}. Then, dividing this by 105 mol e^- per mol N_2 yields R_{N_2}. The constant, 105 mol e^- per mol N_2, is the equivalent of the R_{N_2}/ETS ratio in Codispoti and Packard (1980), 2.4 microL O_2 $L^{-1}h^{-1}$/(gN_2 m^{-3} yr^{-1}). The R_{CO_2} calculation is as follows. R_{CO_2} equals [106/60 mol carbon

(mol N_2)$^{-1}$ $\times$ ETS activity (mol e^- h^{-1} m^{-3})] / [105 mol e^- (mol N_2)$^{-1}$]. The ratio, 106/60 mol C (mol N_2)$^{-1}$, is the Redfield ratio, mentioned above, for the carbon (as CO_2) produced during denitrification from NO_3 (Gruber and Sarmiento, 1997). Note that both R_{O_2} and R_{N_2}, from Table 3 were converted to R_{CO_2} betore being used in the Ez part of Fig. 2a.

2.4 R modelling

To generate R models as depth functions (Table 4), the ETS-based R was plotted against depths (z) normalized by the depth of the R maximum (z_m) as we did in Packard and Christensen (2004). From these plots power functions of the form, R = R_m $(z/z_m)^b$ were fitted to the data using Sigma Plot (version 12.5) according to Charland (2002). Note that R_m is the depth of the respiration maximum and b, the exponent, is always negative. The exponent, b, represents the maximum curvature of the respiration-versus-depth profile. Note that R in the Ez of Fig. 2a is based directly on the ETS measurements (Table 3) while the R in the mesopelagic zone of Fig. 2a is based on the R models in Table 4.

2.5 F_C, NRE , and HEP calculations

The F_C was calculated (Table 2) from depth-normalized water column R (Packard and Christensen, 2004; Packard and Gómez, 2013; Osma et al., 2014). Power functions (R_{CO_2} = R_m $(z/z_m)^b$) were selected over logarithmic or exponential functions because they better described the data as previous studies found (Packard and Christensen, 2004; Packard and Codispoti, 2007). Conceptually, planktonic R_{CO_2} in a seawater cube is considered as equivalent to the difference between the total F_{C_1} through the top of the cube and total F_{C_2} through the bottom of the cube, where total carbon flux refers to the sum of the DOC and the POC carbon flux. We deduce, on the basis of (Craig, 1971; Carlson et al., 2010; Hansell et al., 2012), that R based on DOC and lateral POC flux, compared to the R based on the vertical flux of labile POC, is less than 30% of the total R. Note that if organic matter, in any form, is resistant to oxidation (Arrieta et al., 2015) its flux through the water column will not be detected by respiration measurements. The flux will be transparent to our ETS measurements. However, the dissolved organic matter in the ocean, at least, appears to be oxidizable (Arrieta et al., 2015). In all cases, to a first approximation, one can express our conceptual model by the expression, R_{CO_2} = F_{C_1} - F_{C_2}. In other words, in the vertical, one-dimensional case, the changes in the F_C between depths in a water column are equal to the R_{CO_2} between those depths. Extrapolating this conceptual model to the deep ocean water column, using continuous mathematics, and assuming seafloor carbon burial small, the F_C into the top of a water column (F_{C_t}) can be calculated by integrating all the R below the top boundary (z_t) to the ocean bottom (z_s).

$$F_{C_t} = \int_{z_t}^{z_s} R_{CO_2}\, dz \tag{1}$$

All F_C calculations here are based on depth-normalized power functions of R (R_{CO_2} = R_m (z/z_m)^b, Table 4). (Only if depth is normalized does the equation achieve balance with units of nmol CO_2 min^{-1} L^{-1}). For the carbon flux (F_{f-s}) through any depth layer in the water column (z_f) down to z_s, we use equation 2 and its integrated version in equation 3. Note that these carbon-flux calculations represent the flux at the time the CTD-Niskin cast was made. They are fine scale calculations of C-Flux.

$$F_{f-s} = \int_{z_f}^{z_s} R_{CO_2}\, dz = \int_{z_f}^{z_s} R_m\, (z/z_m)^b\, dz \tag{2}$$

$$F_{f-s} = \{R_m/[(b+1)\, z_m^b]\}\, (z_s^{b+1} - z_f^{b+1}) \tag{3}$$

Note that z_f is any depth between z_t and z_s ($z_t \leqslant z_f \leqslant z_s$) and that F_{f-s} is associated with the microplankton respiration, the greater fraction of water column respiration (Kogelshatz et al., 1978).

The Nutrient Retention Efficiency is equivalent to R (mol CO_2 d^{-1} m^{-3}) within an ocean layer (Δz) divided by the F_C (mol C d^{-1} m^{-2}) into the volume of that layer expressed as a $\%$. Note that the calculation is ($R \times \Delta z$)/F_C. Since the Redfield N/C or P/C ratio is applied to both parts of the ratio, the carbon, N, or P units cancel leaving the ratio unitless. NRE is also the inverse of the carbon flux transfer efficiency (Burd et al., 2010; Buesseler and Boyd, 2009; Buesseler et al., 2007) through the same layer (Packard and Gómez, 2013). For Fig. 2d it was calculated for 20 m layers below the Ez to the ocean bottom from the R models in Table 4 and the F_C models in Table 6.

HEP was calculated from R_{O_2} and R_{N_2}, either derived from the ETS measurements, or from the modeled R_{O_2}, or R_{N_2}. For oxic seawater HEP = $2 \times 2.5 \times 48 \times R_{O_2}$ where 2 represents the number of electron pairs required to reduce O_2 to $2H_2O$, 2.5 represents the ATP/2e$^-$ ratio (Ferguson, 2010), 48 is the ΔG in J per mmol of ATP (Alberty and Goldberg, 1992; Moran et al., 2012), and R_{O_2} in the respiratory O_2 consumption rate as mmol O_2 d^{-1} m^{-3}. For NO_3^- R in anoxic waters HEP = $5 \times 1.0 \times 48 \times R_{N_2}$, where 5 is the number of electron pairs required to reduce NO_3 to N_2, 1.0 is the ATP/2e$^-$ ratio (van Loosdrecht et al., 1997; Smolders et al., 1994), 48 is the ΔG as before, and R_{N_2} in the respiratory NO_3^- reduction rate as mmol N_2 d^{-1} m^{-3}.

3 Results

Oceanographic properties (Table 1) on a C-Line transect at 15°S across the Peru Current upwelling system (Fig.1a) in middle September of the ENSO transition year, 1976, were measured on the R/V Eastward during the JASON-76 cruise of the Coastal Upwelling Ecosystem Analysis (CUEA) JOINT-II expedition. Classic upwelling (Smith, 1968; Packard et al., 1984; Rykaczewski and Checkley, 2008) was evident during this period. Seawater density (σ_t) and NO_3^- sloped surfaceward close

to the coast (Fig. 1b). From 25m (σ_t) rose from 26.0 to 26.1 and NO_3^- rose from 12 to 16 μM. As these dense nutrient-rich waters rose, fertilized the sunlit surface waters at the upwelling center (C3 (Brink et al., 1981; MacIsaac et al., 1985)), and flowed offshore towards C5 and C8, phytoplankton bloomed to 7 mg m^{-3} chlorophyll-a and 18 mg carbon h^{-1} m^{-3} of productivity (Table 1 and Fig. 1b). The dynamics of this process could be seen in the variability of the euphotic zone (Ez) depth. It ranged, from a low of 21 m at C5, the biomass and metabolism maximum position, to twice the depth, 43 m, at the offshore position, C14 (Table 1). Temporal variability was exemplified at the trench position (C12) where over a week, the Ez depth decreased from 40 m to 21 m. Minimal variability occurred at position C8, where over 6 days, the Ez depth remained at 29 m (Table 1). In general, a shallow Ez is caused by high plankton biomass with a high potential for metabolism, and contrary conditions associated with a deep Ez.

Sea surface R_{O_2} ranged six-fold from a low of 24.1 μmol O_2 m^{-3} h^{-1} at the upwelling center to a high of 144.7 μmol O_2 m^{-3} h^{-1}, 93 km offshore at the trench position, C12 (Table 1). Within days, R_{O_2} could change 3-fold both inshore and offshore (Table 3). During the week between C3 stations 15 and 21, R_{O_2} rose from 24.1 to 84.0 μmol O_2 m^{-3} h^{-1} and R_{O_2} at C12 rose from 47.1 μmol O_2 m^{-3} h^{-1} (station 17) to 144.7 μmol O_2 m^{-3} h^{-1} (station 35, Table 2). This high respiration (R) at station (sta) 35, occurred in a diatom bloom of *Chaetoceros compressus* and *Ch. lorenzianus*. Such temporal variability in seawater R_{O_2} is just beginning to be documented (Fernández-Urruzola et al., 2014; Osma et al., 2014). Similar increases were seen in the chlorophyll and net productivity at C3 and C12 (Table 1). The co-occurrence of this rise in R_{O_2}, chlorophyll and net productivity suggests seawater R_{O_2} being driven by phytoplankton. Below the immediate sea surface, microplankton R_{O_2} usually increased to a subsurface maximum within the Ez and then decreased dramatically towards the bottom of the Ez and into the dark ocean below (Table 2 and S3). R_{CO_2} (Fig. 2a) ranged in the Ez from 0.4 mmol CO_2 m^{-3} d^{-1} in the upwelling center (C3, sta 15) to 3 mmol CO_2 m^{-3} d^{-1} at C5, the shelf edge sta 20. The lowest epipelagic R_{CO_2} (Table 5) compares with the R_{CO_2} range of 22-27 mmol CO_2 m^{-2} d^{-1} reported recently in eddy-upwelling in the South China Sea (Jiao et al., 2014). In the denitrifying waters R_{CO_2} was in the μmol range with a low of 4 μmol CO_2 m^{-3} d^{-1} at C5 (sta 37) to 133 μmol CO_2 m^{-3} d^{-1} at C3 (sta 21). In the mesopelagic waters below 500m (Table 5) R_{CO_2} ranged from 0.4 to 6.1 μmol CO_2 m^{-3} d^{-1} over a week at C-Line position C8, at other locations R_{CO_2} fell in between this range. Deeper in the water column, over the trench and beyond, bathypelagic R_{CO_2} ranged from 0.3 μmol CO_2 m^{-3} d^{-1} at C10 over the trench to 3.7 μmol CO_2 m^{-3} d^{-1} at C8 over the continental slope (Table 5). Benthic R_{CO_2} and C burial (Table 5 and Fig. 3a) ranged from a high of 90 mmol CO_2 m^{-2} d^{-1} at C3, the upwelling center, to a low of 0.09 mmol CO_2 m^{-2} d^{-1} at trench position, C10, with a depth of 4300 m. The R_{CO_2} section in Fig. 2a shows clearly the strength of R and its associated remineralization in the upper 50 m of the water column and a tongue of high R descending deeper into the water column at position C8 50 km off the coast. F_C along the C-Line transect is shown in Fig 2b. In order to include the inshore stations,

F_C, in Fig. 2b, only represents that part of the C-flux that supports the water column respiration. It does not include benthic R and C burial. To scale our F_C calculations, F_C at 150m, seaward of C8, ranged from 3 to 6 mmol CO_2 m^{-3} d^{-1} (Table 6). These fluxes are comparable to the range of 2.5 to 6.2 mmol CO_2 m^{-3} d^{-1} recently measured at 100 m by (Jiao et al., 2014).

As one would expect with strong F_C at C8, even at 1000 m, the carbon flux transfer efficiency (T_{eff}, Buesseler et al. (2007)) at this station (19) is high and the NRE low (Table 6, Fig. 3b). T_{eff} between 150 and 500 m ($T_{eff_{500}}$) is 82 and the NRE is only 18 $\%$ (Table 6). Ironically, despite the decrease in F_C throughout the water column at C8 between 17 and 23 September, $T_{eff_{500}}$ only decreased by less than a factor of 2 to 45 $\%$ (Table 6). The impact on the NRE was greater, increasing 3 fold to 55 $\%$ (Table 6). $T_{eff_{500}}$ at other locations ranged from 28 at C10 to 47 at C14 (Fig. 3b). In addition to this unique documentation of the temporal variability of F_C from Table 5, Fig. 2b demonstrates its mesoscale spatial variability. That transect shows a maxima occurring throughout the water column, 50 km from the coast at the upper slope position, C8. As Table 5 and Fig. 3a show, the benthic R and burial are also high at this location. Fig. 3b highlights the importance of the maximum curvature of the respiration-depth profile. As |b| increases towards 2 the NRE increases towards 70$\%$ and the $T_{eff_{150-500}}$ decreases towards 30$\%$.

HEP in the Ez (Fig 2d and Table 7) ranges from a high of 555 J d^{-1} m^{-3} at the R maximum at C5 (sta 20) to a low of 69 J d^{-1} m^{-3} at the bottom of the Ez at C3 (sta 21). It drops slightly over the continental slope, but further offshore over the trench (C12) high values of 880 J d^{-1} m^{-3} can be found (Fig 2d). In the far offshore the Ez HEP only reaches values of 315 J d^{-1} m^{-3}. As examples of low HEP values, at 4755 m in the trench it decreases to 0.02 J d^{-1} m^{-3}. Thus the range of HEP by all the respiratory ETS and oxidative phosphorylation coupling in the microplankton of this part of the Peru current upwelling system spans 4 orders of magnitude from 0.02 J d^{-1} m^{-3} in the abyssalpelagic waters of the trench to 880 J d^{-1} m^{-3} in the Ez above. This is the first time such calculations have been made. Integrating the epipelagic HEP (Table 7) over the upper 150 m yields a range from a low of 6.6 x 10^{-3} MJ d^{-1} m^{-2} to a high of 0.39 MJ d^{-1} m^{-2}, averaging 0.09 MJ d^{-1} m^{-2}. This average HEP is only 0.7 $\%$ of the average solar radiation (13.5 $\pm$ 4.0 MJ d^{-1} m^{-2}) at the C-Line sea surface between Sept 12-24 during the JASON-76 cruise (Packard and Jones, 1976).

4 Discussion

Here we have demonstrated the calculation of R_{CO_2}, F_C, NRE, and HEP in an ocean section from microplankton ETS activity measurements. We have previously explained how ocean water column R_{CO_2} determines F_C of labile organic matter by oxidizing sinking POC and mineralizing phosphate and nitrate (Osma et al., 2014; Packard and Codispoti, 2007). Fig. 3b shows that the maximum curvature of the respiration-depth profile determines NRE as well as F_C transfer efficiency. The offshore R_{CO_2} section (Fig. 2a) shows the variability of R with depth and location in the upwelling

area. Fig.2a also shows how seawater respiration is displaced seaward to C8 from the chlorophyll maximum at C5 (Fig. 1b). The F_C section (Fig. 2b) demonstrates the power of using R to calculate spatial variability of F_C by revealing a F_C maximum over the upper part of the continental slope. The NRE section (Fig. 2c) reveals its inverse relationship to F_C as well as its variability in the water column. This ability of the water column to retain nutrients would not have been detected without the original ETS activity profiles. The HEP section (Fig. 2d) showing the energy production by the ATPases in microbial mitochondrion and plasmalemma membranes of bacteria and archaea in the water column is a new representation of ATP production in oceanographic analysis. Because a major purpose of all forms of respiration is to make ATP, HEP should reflect R_{CO_2} in any section or profile. The similarity of the R_{CO_2} pattern in Fig. 2a and the HEP pattern in Fig. 2d shows that it does.

Ocean R_{CO_2} filters sinking labile POC and should vary inversely with benthic R and carbon burial. However, the relationship between the two variables is more complicated (Figs. 2a and 3a). We can see this in the R maximum 50 km off the Peru coast at C-Line position C8. One might expect low benthic R and carbon burial here (Table 5), but that is not the case (Fig. 3a). From the difference between integrating the R function (Eq. 2) to infinity and integrating it to the ocean bottom (z = s) we calculate a high level of benthic R and carbon burial (Fig. 3a). The minimum NRE at C-Line position, C8, in Fig. 2c explains this discrepancy. The delivery of labile POC to the bottom depends, not directly on F_C, but on the ratio of the water column R (Fig. 2a) to F_C (Fig. 2b). Recent studies of the organic carbon preservation on the upper parts of the Peruvian continental slope (Dale et al., 2014) support these calculations of high carbon burial (Fig 3a.) They find high burial rates at depths between 200-400m (the upper part of the Peruvian continental slope) and attribute it to the anoxia overlying these sediments. A C-Line section of the T_{eff}, the inverse of the NRE, it would have revealed a T_{eff} maximum at C8. One can deduce this from Fig. 3b.

ETS measurements can be used, not only to calculate F_C, NRE, and HEP, but also to calculate biological heat production (Pamatmat et al., 1981), age, and flow rates of deep and bottom waters (Packard, 1985a). In anoxic waters, if the background chemistry (Richards, 1965; Packard, 1969) is known, ETS measurements provide proxy rate measurements for denitrification (Codispoti and Packard, 1980; Dalsgaard et al., 2012), NO_2^- production, nitrous oxide production, and sulfide production (Packard et al., 1983), and even for iron and magnesium reduction rates (Lane et al., 2010). All are different forms of R, but all are controlled by the same basic respiratory ETS with NADH-dehydrogenase (Complex 1) as the common gate-keeper. Furthermore, because the energy generation of nitrification is based on a variation of this ETS, an ETS measurement is also likely a proxy for nitrification.

HEP, as ATP generation in the ocean water column, could have been calculated from R_{O_2} since 1943, the time the Nobelist, Severo Ochoa first established the connection between ATP production and R (Ochoa, 1943). However, until Fig. 2d, calculations of biological energy production, including HEP, in the ocean have not been made (Karl, 2014). Now the time is more propitious to make such

calculations with recent research (Lane, 2002, 2005, 2009; Wilson et al., 2012; Chen and Strous, 2013) documenting the ubiquity of respiratory ETS in the biosphere, how it relates to R_{O_2}, to all other ocean respiratory processes, and to HEP as ATP production. As we have seen above, HEP and R_{CO_2} in the Peru upwelling system have similar time and space distributions (Figs. 2a and d). The small difference in the ATP/2e$^-$ relationships between oxidative phosphorylation and the rate of electron transfer in aerobic metabolism and denitrification has minimal impact. In aerobic metabolism the ATP/2e$^-$ ratio is 2.5; in denitrifying microbes ATP/2e$^-$ is 1.0 (van Loosdrecht et al., 1997; Smolders et al., 1994). At the rate anammox research is progressing (Dalsgaard et al., 2012), its relative contribution will soon be known, too. In any case, less ATP should be produced in anoxic waters resulting in a lower HEP. It will be interesting in the future to look for this difference by comparing HEP offshore sections made through oxic and anoxic sectors of upwelling systems.

5 Conclusions

Organic carbon fluxes are critical component of reliable carbon budgets, but they are so difficult to measure that rarely can enough measurements be amassed to construct a synoptic section of F_C. Here, from plankton respiration models we present an original mode of calculating F_C sections as well as benthic respiration and carbon burial. We reveal the importance of plankton respiration in determining the capacity of a plankton community in retaining water column nutrients, develop the concept of Nutrient Retention Efficiency (NRE), and demonstrate NRE variability in an ocean section. In addition, we show that the curvature of the respiration profile (the exponent, b, of the power function) controls both the NRE and F_C. Finally, we use respiration to calculate the heterotrophic energy production (HEP), the rate of ATP generated by plankton metabolism and find an HEP maximum over the shelf break on the upper part of the Peruvian continental slope.

Acknowledgements. We thank, J Ammerman, RT Barber, D Blasco, RC Dugdale, N Garfield, and J Kogelschatz, for their collaboration. D. Bourgault revealed the role of depth-normalization. The challenges from the three reviewers led to many improvements in this paper and for their diligence we are thankful. NSF (USA) Grant OCE 75-23718A01 (TTP) funded JASON-76. The Basque Government (NO and I F-U), MEC (Spain) project BIOMBA, CTM2012-32729/MAR (MG), and CIE (Canary Islands):Tricontinental Atlantic Campus (TTP) funded analysis.

References

Alberty, R. and Goldberg, R.: Standard thermodynamic formation properties of adenosie 5'-triphosphate series, Biochem, 31, 10 610–10 615, 1992.

Arístegui , J., Gasol, J., Duarte, C., and Herndl, G.: Microbial oceanography of the dark ocean's pelagic realm, Limnol. Oceanogr, 54, 1501–1529, 2009.

Arrieta, J., Mayol, E., Hansman, L., Herndl, G., Dittmar, T., and Duarte, C.: Dilution limits dissolved organic carbon utilization in the deep ocean, Science, (1258955), 2015.

Barber, R., Dugdale, R., MacIsaac, J., and Smith, R.: Variations in phytoplankton growth associated with the source and conditioning of upwelling water, Investig. Pesq, 35 (1), 171-193, 1971.

Barber, R., Huntsman, S., Kogelschatz, J., Smith, W., and Jones, B.: Coastal Upwelling Ecosystems Analysis. Data Report 49. Carbon, Chlorophyll and Light Extinction from JOINT II, vol. 49, CUEA Data Rep, 1978.

Brink, K., Jones, B., Vanleer, C., Mooers, C.,Stuart, D., Stevenson, M., Dugdale, R., and Heburn, G.: Physical and biological structure and variability of the upwelling center off Peru at 15∘S, during March 1977: Coastal Upwelling. Coastal and estuarine sciences 1, vol. xi–xiii, ed Richards FA (American Geophysiscal Union, Wasington DC), p. 473-495, 1981.

Buesseler, K. and Boyd, P.: Shedding light on precesses that control particle export and flux attenuation in the twilight zone of the open ocean, Limnol Oceanogr, 54, 1210–1232, 2009.

Buesseler, K., Lamborg, C., Boyd, P., Lam, P., Trull, T., Bidigare, R., Bishop, J., Casciotti, K., Dehairs, F., Elskens, M., Honda, M., Karl, D., Siegel, D., Silver, M., Steinberg, D., Valdes, J., Mooy, V., B, W., and S: Revisiting carbon flux through the ocean's twilight zone, Science, 316, 567–570, 2007.

Burd, A., Hansell, D., Steinberg, D., Anderson, T., Arístegui, J., Baltar, F., Beaupré, S., Buesseler, K., Dehairs, F., Jackson, G., Kadko, D., Koppelmann, R., Lampitt, R., Nagata, T., Reinthaler, T., Robinson, C., Robison, B., Tamburini, C., and Tanaka, T.: Assessing the apparent imbalance between geochemical and biochemical indicators of meso- and bathypelagic biological activity What the @$?! is wrong with present calculations of carbon budgets?, Deep-Sea Res II, 57, 1557–1571, 2010.

Carlson, C., Hansell, D., Nelson, N., Siegel, D., Smethie, W., Katiwala, S., Meyers, M., Halewood, E.: Dissolved organic carbon export and subsequent remineralization in the mesopelagic and bathypelagic realms of the North Atlantic basin, Deep-Sea Res II, 57, 1433–1445, 2010.

Charland, M.: SigmaPlot 2000/2001 for Scientists, Riparian House Merrickville (Ontario), 2002.

Chen, J. and Strous, M.: Denitrification and aerobic respiration, hybrid electron transport chains and co-evolution, Biochim. Biophys. Acta, 1827, 136-144, 2013.

Christensen, J.P. and Packard, T.: Respiratory electron transport activities in plankton: comparison of methods, Limnol. Oceanogr, 24 (3), 576-583, 1979.

Christensen, J., Packard, T., Dortch, Q., Minas, H., Garfield, P., and Richez, C.: Carbon oxidation in the deep Mediterranean Sea: evidence for dissolved organic carbon source, Global Biogeochem. Cycles, 3 (4), 315-335, 1989.

Cleland, W.: Enzyme kinetics, Ann Rev Biochem, 36.1, 77-112, 1967.

Codispoti, L. and Packard, T.: Denitrification rates in the Eastern tropical South Pacific, J Mar Res, 38, 453–477, 1980.

Codispoti, L., Brandes, J., Christensen, J., Devol, A., Naqvi, S., Paerl, H., and Yoshinari, T.: The oceanic fixed nitrogen and nitrous oxide budhets: Moving targets as we enter the anthropocene?, Sci Mar, (Suppl 2), pp. 85–105, 2001.

Codispoti, L., Dugdale, R., and Minas, A.: A comparison of the nutrient regimes off northwest Africa, Peru and Baja California, Rapp. P. Reun. Cons. Int. Explor. Mer, 180, 184- 201, 1982.

Craig, H.: The deep metabolism: oxygen consumption in abyssal ocean water, J Geophys Res, 76, 5078–5086, 1971.

Dale, A., Sommer, S., Lomnitz, U., Montes, I., Treude, T., Gier, J., Hensen, C., Dengler, M., Stolpovsky, K., Bryant, L., and Wallmann, K.: Organic carbon production, mineralization and preservation on the Peruvian margin, Biogeosciences Discuss.,11, 13067?13126, 2014.

Dalsgaard, T., Thamdrup, B., Farías, L., and Revsbech, N.: Anammox and denitrification in the oxygen minimum zone of the eastern South Pacific, Limnol Oceanogr, 57, 1331–1346, 2012.

Ducklow, H. and Doney, S.: What is the metabolic state of the oligotrophic ocean? A debate, Annu Rev Mar Sci, 5, 525–533, 2013.

Eppley, R. and Peterson, B.: Particulate organic matter flux and planktonic new production in the deep ocean, Nature, 282, 677-680, 1979.

Ferguson, S.: ATP synthase: From sequence to ring size to the P/O ratio, Proc Nati Acad Sci USA, 107, 16 755–16 756, 2010.

Fernández, C., Faría, L., and Alcaman, M.: Primary production and nitrogen regeneration processes in surface waters of the Peruvian upwelling system, Prog Oceanogr, 83, 159–168, 2009.

Fernández-Urruzola, I., Osma, N., Packard, T., Gómez, M., and Postel, L.: Distribution of zooplankton biomass and potential metabolic activities across the northern Benguela upwelling system, J Mar Syst, 2014.

Garfield, P., Packard, T., and Codispoti, L.: Particulate protein in the Peru upwelling system, Deep-Sea Res, 26, 623–639, 1979.

Giering, S., Sanders, R., Lampitt, R., Anderson, T., Tamburini, C., Boutrif, M., Zubkov, M., Marsay, C., Henson, S., Saw, K., Cook, K., and Mayor, D.: Reconciliation of the carbon budget in the ocean's twilight zone, Nature, 2014.

Gruber, N. and Sarmiento, J.: Global patterns of marine nitrogen fixation and denitrification, Glob Biogeochem Cycles, 11, 235–266, 1997.

Hafferty, A., Codispoti, L., and Huyer, A.: JOINT-I1 R/V Melville Legs I, I1 and IV WV Iselin Leg I1 bottle data March 1977-May 1977,, 45, CUEA Data Rep, 1978.

Hansell, D., Carlson, C., and Schlitzer, R.: Net removal of major marine dissolved organic carbon fractions in the subsurface ocean, Glob Biogeochem Cycles, 26 (GB1016),m doi:10.1029/2011GB004069, 2012.

Harvey, H.: The Chemistry and Fertility of Sea Waters. (Cambridge University Press, Cambridge), p. 224, 1955.

Jenkins, W.J.: Oxygen utilization rates in North Atlantic subtropical gyre and primary production in oligotrophic systems, Nature, 300, 246–248, 1982.

Jenkins, W.J.: The use of tracers and water masses to estimate rates of respiration, Heterotrophic Activity in the Sea, 391-403., eds Hobbie, J.M., Williams, P.J.Le B. (Plenum Press, New York), 1984.

Jiao, N., Zhang, Y., Zhou, K., Li, Q., Dai, M., Liu, J., Guo, J., and Huang, B.: Revisiting the CO_2 problem in upwelling areas-a comparative study on eddy upwellings in the South China Sea, Biogeosciences, 11, 465–2475, 2014.

Karl, D.M.: Solar energy capture and transformation in the sea, Elem Sci Anthro, 2, 1–6, 2014.

Kenner, R. and Ahmed, S.: Measurements of electron transport activity in marine phytoplankton, Mar Biol, 33, 119–127, 1975.

King, F., Devol, A., and Packard, T.: On plankton biomass and metabolic activity from the eastern tropical North Pacific, Deep-Sea Research, 25, 689-704, 1985.

King, L.: The coastal upwelling ecosystems analysis program as an experience in international cooperation, Ocean Dev & Int'l L, 9, 269–288, 1981.

Kogelshatz, J., Shepherd, R., Whitledge, T., Codispoti, L., and Huyer, A.: JOINT-II JASON 76 hydro data. R/V EASTWARD Cruises E-5F-76 through E-5L-76, vol. 38, International Decade of Ocean Exploration, CUEA Data Rep, 1978.

LaFerla, R., Azzaro, M., Civitarese, G., and Ribera d'Alcala, M.: Distribution patterns of carbon oxidation in the eastern Mediterranean Sea: evidence of changes in the remineralization processes, J Geophys Res, 108 (C9), 8111, 2003.

Lane, N., Allen, J., and Martin, W.: How did LUCA make a living? Chemiosmosis in the origin of life, BioEssays, 32, 271–280, 2010.

Lane, N.: The Molecule that made the World, OUP (Oxford), p. 384, 2002.

Lane, N.: Power, Sex, Suicide: Mitochondria and the Meaning of Life, OUP (Oxford), p. 368, 2005.

Lane, N.: Life Ascending: The Ten Great Inventions of Evolution, OUP (Oxford), p. 352, 2009.

Laufkötter, C., Vogt, M., and Gruber, N.: Long-term trends in ocean plankton production and particle export between 1960-2006, Biogeosciences, 10, 7373–7393, 2013.

Lotka, A.: Elements of physical biology, eds Williams & Wilkins Company (Baltimore), 1925.

MacIsaac, J., Dugdale, R., Barber, R., Blasco, D, and Packard, T.: Primary production cycle in an upwelling center, Deep-Sea Res., 32, 503-529, 1985.

Madigan, M., Martinko, J., Parker, J.: Brock Biology of Microorganisms, Prentice Hall, Upper Saddle River, New Jersey,p. 991, 2000.

Martin, J.H., Knauer, G.A., Karl, D.M., Broenkow, W.W.: VERTEX: carbon cycling in the northeast Pacific, Deep-Sea Res, 34 (2), 267-285,1987.

Minas, J., Codispoti, L., Dugdale, R.: Nutrients and primary production in the upwelling region off northwest Africa, Rapp. P. Reun. Cons. Int. Explor. Mer, 180, 148-183,1982.

Moran, L., Horton, R., Scrimgeour, K., and Perry, M.: Principles of Biochemistry, 2012.

Munk, W.: Abyssal Recipes, 13, 707-730,1966.

Nelson, D. and Cox, M.: Lehninger Principles of Biochemistry, Worth Publishers, New York, p. 1152, 2000.

Ochoa, S.: Efficiency of aerobic phosphorylation in cell-free heart extracts, J Biol Chem, 151, 493–505, 1943.

Odum, H.T.: Primary production in flowing waters, Limnol Oceanogr, 1, 102–117, 1956.

Osma, N., Fernández-Urruzola, I., Packard, T., Postel, L., Gómez, M., and Pollehne, F.: Short-term patterns of vertical particle flux in northern Benguela: a comparison between sinking POC and respiratory carbon consumption, J Mar Syst, 2014.

Packard, T.: The estimation of the oxygen utilization rate in seawater from the activity of the respiration electron transport system in plankton, Ph.D. Thesis, University of Washington, Seattle, 1-115, 1969.

Packard, T.: Organizers remarks: Coastal Upwelling. Coastal and estuarine sciences 1, vol. xi–xiii, ed Richards FA (American Geophysiscal Union, Wasington DC), 1981.

Packard, T.: Oxygen consumption in the ocean: Measuring and mapping with enzyme analysis. Mapping strategies in chemical oceanography ed Zirino A Advances in Chemistry. American Chemical Society, Washington DC, p. 178-209,1985.

Packard, T.: Measurement of electron transport activity of marine microplankton. Advances in Aquatic Microbiology eds Williams LeB. and Jannasch H. Academic, New York, p. 207-261,1985.

Packard, T. and Christensen, J.: Respiration and vertical carbon flux in the Gulf of Maine water column, J Mar Res, 62, 93–115, 2004.

Packard, T. and Codispoti, L.: Respiration, mineralization, and biochemical properties of the particulate matter in the southern Nansen Basin water column in April 1981, Deep-Sea Res I, 54, 403–414, 2007.

Packard, T. and Gómez, M.: Modeling vertical carbon flux from zooplankton respiration, Prog Oceanogr, 110, 59–68, 2013.

Packard, T. and Jones, V.: Biochemistry and ecology of the Peru Current: The JASON expedition to the Peru upwelling system, September 1976, CUEA Tech Rep, 46, 129, 1976.

Packard, T. and Williams, P. LeB.: Rates of respiratory oxygen consumption and electron transport in surface seawater from the Northwest Atlantic Ocean , Oceanologica Acta, 4 (3), 351-358, 1981.

Packard, T., Blasco, D., and Dugdale, R.: Coastal Upwelling: A short summary of its physical, chemical and biological characteristics. Marine Geology and Oceanography of Arabian Sea and Coastal Pakistan, eds Haq, B., Milliman, J. (Van Nostrand Reinhold, New York), p. 339-350, 1984.

Packard, T., Denis, M., Rodier, M., and Garfield, P.: Deep-ocean metabolic CO2 production: calculations from ETS activity., Deep-Sea Res I, 35, 371-382, 1988.

Packard, T., Garfield, P., and Codispoti, L.: Oxygen consumption and denitrification below the peruvian upwelling. Coastal upwelling: Its sediment record, vol. 147–173., , eds Suess, E., Thiede, J. (Plenum Press, New York), 1983.

Packard, T., Healy, M., and Richards, F.: Vertical distribution of the activity of the respiratory electron transport system in marine plankton, Limn Oceanogr, 16, 60–70, 1971.

Pamatmat, M., Graf, G., Bengtsson, W., and Novak, C.: Heat production, ATP concentration and electron transport activity of marine sediments, Mar Ecol Prog Ser, 4, 135-143, 1981.

Redfield, A., Ketchum, B., and Richards, F.: The influence of organisms on the composition of seawater, Pp. 26-77. In Hill, N. M. (Ed), The Seas vol II, Interscience New York, 1963.

Richards, F.: Oxygen in the Ocean, In Hedgepeth, J W. (Ed). Treatise on Marine Ecology and Paleoecology. Geol Soc America 67 (1), 1957.

Richards, F.: Anoxic Basins and Fjords. Chemical Oceanography, eds Riley JP, Skirrow, G (Academic Press, New York), 1965.

Richards, F.: Coastal upwelling, American Geophysical Union (Washington, DC), p. 529, 1981.

Riley, G.: Oxygen, phosphate, and nitrate in the Atlantic Ocean , Bingham Oceanogr. Collection Bulletin, 13 (3), 1-169, 1951.

Rykaczewski, R. and Checkley, D.: Influence of ocean winds on the pelagic ecosystem in upwelling regions., PNAS, 105 (6), 1065?1970, 2008.

Ryther, J., Menzel, D., Hulburt, E., Lorenzen, C., and Corwin, N.: Production and utilization of organic matter in the Peru Coastal Current, Anton Brun Rep, 4, 4.3–4.12, 1970.

Santoso, A., McGregor, S., Jin, F., Cai, W., England, M., An, S., McPhaden, M., and Guilyardi, E.: Late-twentieth-century emergence of the El Niño propagation asymmetry and future projections, Nature, 504, 126–130, 2013.

Schatteman, G., Gibbs, L., Lanahan, A., Claude, P., and Bothwell, M.: Expression of NGF receptor in the developing and adult primate central nervous system, J Neuroscience, 8.3, 860-873, 1988.

Seiwell, H.: The distribution of oxygen in the western basin of the North Atlantic, Papers in Phys. Ocean. and Meteorol, VoL. IIi, (1) p. 1-86, 1934.

Seiwell, H.: Consumption of oxygen in seawater under controlled laboratory conditions, Nature, 140, 506-507, 1937.

Sigman, D., Altabet, M., Michener, R., McCorkle, D., Fry, B., and Holmes, R.: Natural abundance-level measurement of the nitrogen isotopic composition of oceanic nitrate: an adaptation of the ammonia diffusion method, Mar Chem, 57(3), 227-242, 1997.

Smith, R.: Upwelling, Oceanogr. Mar. Biol. Annu. Rev., 6, 11?46, 1968.

Smolders, G., der Meij, V., J, V. L., MCM, H., and JJ: Stoichiometric model of the aerobic metabolism of the biological phosphorus removal process, Biotech Bioeng, 44, 837–848, 1994.

Suess, E.: Particulate organic carbon flux in the oceans-surface productivity and oxygen utilization, Nature, 288, 260–263, 1980.

Takahashi, T., Broecker, W., and Langer, S.: Redfield ratio based on chemical data from isopycnal surfaces, J Geophys Res, 90, 6907–6924, 1985.

van Loosdrecht, MCM, S., GJ, K., T, H., and JJ: Metabolism of micro-organisms responsible for enhanced biological phosphorus removal from wastewater, Antonie Leeuwenhoek, 71, 109–116, 1997.

Walker, J.: ATP synthesis by rotary catalysis, Angew chem int ed, 37, 2308–2319, 1998.

Walsh, J.: Implications of a systems approach to oceanography, Science, 176, 969-975, 1972.

Walsh, J., Kelly, J., Dugdale, R., and Frost, B.: Implications of a systems approach to oceanography, Gross features of the Peruvian upwelling system with special reference to possible diel variation, Invest. Pesq. 35 (1), 25-42, 1971.

Watt, N., Montgomery, M., Runswick, M., Leslie, A., and Walker, J.: Bioenergetic cost of making an adenosine triphosphate molecule in animal mitochondria, 2010.

Williams, P., Quay, P., Westberry, T., and Behrenfeld, M.: The oligotrophic ocean is autotrophic, Annu Rev Mar Sci, pp. 16.1–16.15, 2012.

Wilson, S., Kolber, Z., Tozzi, S., Zehr, J., and Karl, D.: Nitrogen fixation, hydrogen cycling, and electron transport kinetics in trichodesmium erythraeum (cyanobacteria) strain ims1011, J. Phycol. 48 (3), 595-606, 2012.

Wooster, W.: Yearly changes in the Peru Current, Limnol Oceanogr, 6, 222–226, 1961.

Wyrtki, K.: Circulation and water masses in the Eastern equatorial Pacific Ocean, Int J Oceanol Limnol, 1, 117–147, 1967.

Zheng, Y, Schlosser, P., Swift, J., and Jones, E.: Oxygen utilization rates in the Nansen Basin, Arctic Ocean: implications for new production, Deep Sea Res, 144, 1923?1943, 1997.

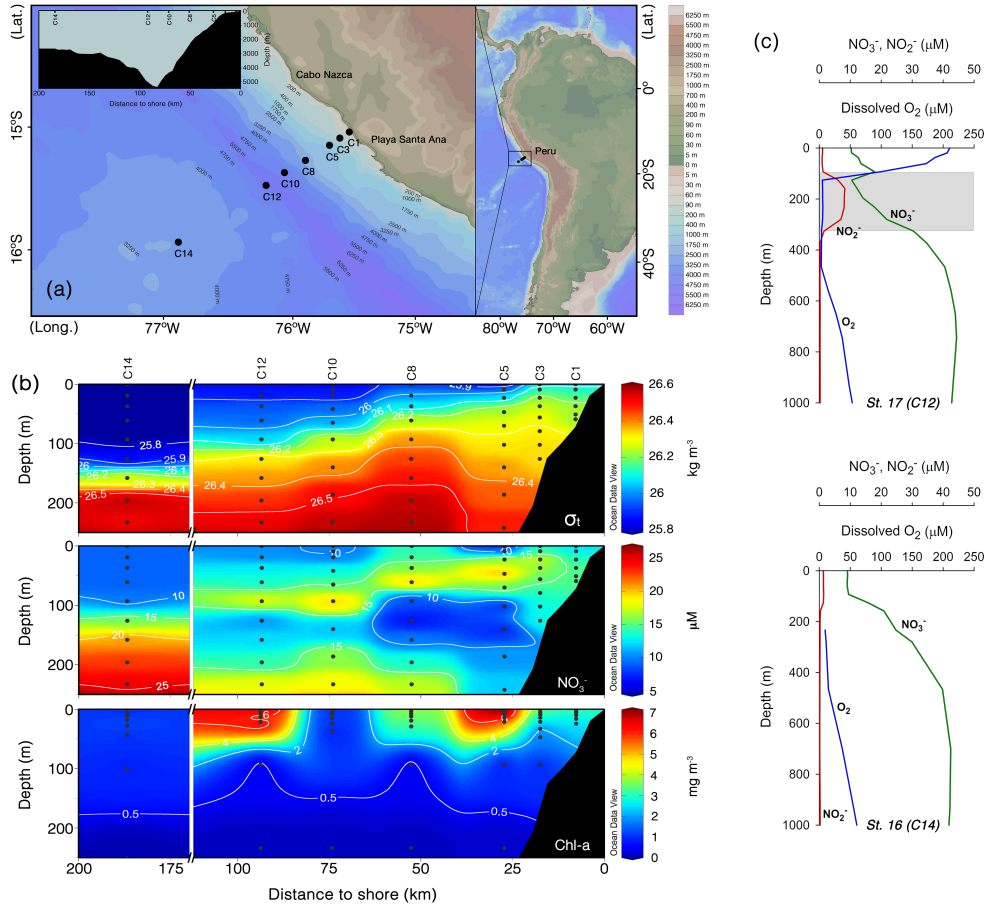

Figure 1. (a) C-line section orthogonal to the Peru coast at 15°S. The innermost C-Line position, C1, was 2.7 km from the coast between Cabo Nazca and Punta Santa Ana. The outermost position, C14, was located west of the Peru-Chili trench 185.2 km from the coast. Depth along this transect ranged from 63 m at C1 to 4755 m at C12. C14 was in 2680m of water on the gently rising abyssal plain seaward of the trench (inset upper left). (b) Density (σ_t), NO_3^- (μM units) and phytoplankton chlorophyll (mg m^{-3}) sections along the C-line from C1 to C14 (top, middle and bottom panels, respectively). All sections represent the upwelling from 13 to 20 September 1976. Scale brakes avoid interpolation over a 90 km data gap. The high phytoplankton biomass over the shelf break occurs between C5 and C8, 15 to 35 km from the coast. (c) NO_3^-, NO_2^-, and O_2 depth profiles through the mesopelagic waters over the Trench at C12 (top) and over the outermost station at C14 (bottom). The vertical plot at C12 documents the first step in denitrification (shaded area), NO_3^- reduction to NO_2^-, at the foot of the oxycline, in the OMZ between 150 and 300 m. In contrast, the vertical profiles at C14, 185 km off the coast, show the absence of denitrification in mesopelagic waters.

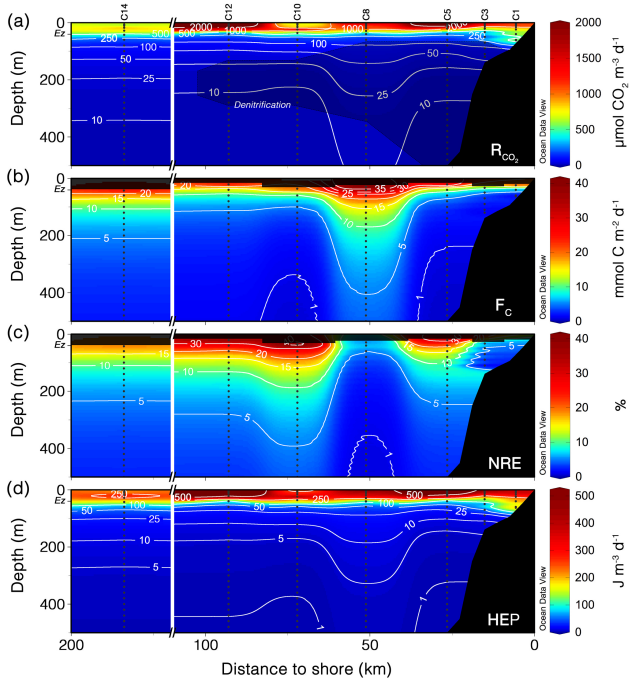

Figure 2. Sections for the upper 500 m along the C-line. (a) R_{CO_2}; the dark shadow delimits denitrification in the OMZ. In the Ez, R_{CO_2} is calculated directly from ETS-based R_{O_2} (Table 3). In the mesopelagic waters below, R_{CO_2} is modeled from the respiration equations in Table 4. (b) F_C is calculated by integration of the respiration models (Table 4) to the ocean bottom according to the equations [2] and [3]. (c) NRE, as a %, is determined from models in Tables S4 and S6 as $100\times(R_{CO_2}/F_C)$. (d) HEP is either derived directly from ETS activity in the surface waters or from modeled R_{O_2} or R_{N_2} for depths below the Ez (as in Fig. 2a).

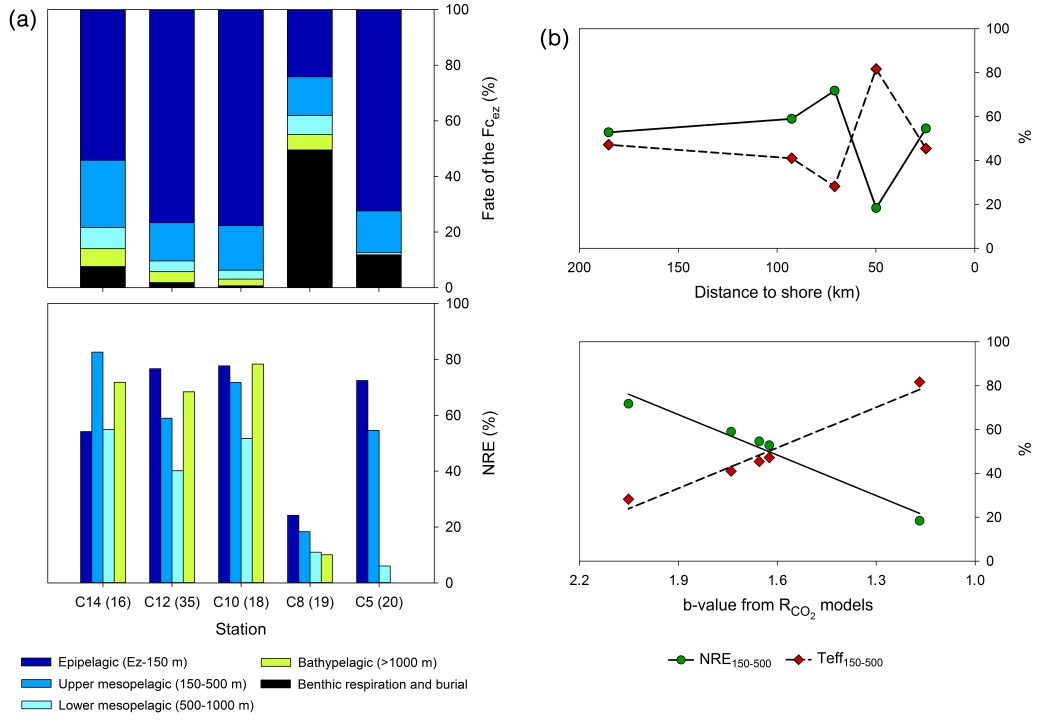

Figure 3. (a) Fate of the carbon fluxing out of the Ez (Fc$_{ez}$) into the water column and seafloor below (as a % of the total flux) along the C-Line (top panel). In the water column, the carbon is remineralized through R. In the benthos, part is remineralized and returned to the water column above and part is buried. Bottom panel shows the different efficiencies with which carbon is remineralized through respiration in 4 different zones of the water column along the C-Line. (b) Top panel: variability of the NRE and the T$_{eff}$ in the upper mesopelagic waters (150-500 m) along the C-line. Bottom panel: NRE and T$_{eff}$ as a function of the maximum curvature *b* (absolute value) in the R$_{CO_2}$ models from Table 4.

Table 1. Oceanographic characteristics of Peru upwelling C-Line stations during Duke University's JASON-76 R/V Eastward cruise E-5H-67. Euphotic zone depth is the 1% light level. Original data are in CUEA Data Reports (Kogelshatz et al., 1978; Packard and Jones, 1976).

CUEA C-Line Position (JASON Station)	Coordinates	Date in Sept 1976	Distance to coast (km)	Ocean depth (m)	Surface temperature (°C)	Surface salinity (PSU)	Euphotic zone (m)	Surface chlorophyll (mg m^{-3})	Surface respiration (μmol O_2 m^{-3} h^{-1})	Surface net productivity (mg C m^{-3} h^{-1})
C1 (22)	15°03.2'S 75°26.0'W	20	2.7	63	14.28	34.902	24	3.06	56.11	6.84
C3 (15)	15°05.9'S 75°31.4'W	12	12.9	117	14.26	-	42	2.09	24.11	3.67
C3 (21)	15°06.5'S 75°31.0'W	19	12.9	120	14.10	34.869	33	3.67	83.99	8.08
C5 (20)	15°09.9'S 75°35.7'W	18	24.7	500	15.59	34.921	21	6.96	119.13	18.24
C5 (37)	15°10.5'S 75°36.2'W	24	24.7	607	15.00	34.921	27	3.77	79.97	8.88
C8 (19)	15°16.9'S 75°47.8'W	17	49.9	1880	14.97	34.902	29	4.11	80.32	9.65
C8 (36)	15°16.9'S 75°14.8'W	23	49.9	2150	16.10	35.069	29	3.90	87.67	12.35
C10 (18)	15°22.0'S 75°59.8'W	16	70.9	4300	15.92	35.077	36	1.06	34.35	1.64
C12 (17)	15°28.0'S 76°08.0'W	15	92.6	4000	15.75	35.046	40	1.14	47.14	1.93
C12 (35)	15°29.0'S 76°07.8'W	22	92.6	4755	15.46	34.950	21	7.47	144.71	16.64
C14 (16)	15°55.8'S 76°51.6'W	13	185.2	2680	16.48	35.147	43	0.92	40.90	1.63

Table 2. Step-by-step calculations of F_C from ETS activity at C-Line position C12 (station 35). Potential aerobic R (Φ), R_{O_2}, N_2 production from denitrification (R_{N_2}) and respiratory CO_2 production (R_{CO_2}) were first determined from temperature-corrected ETS activity values. Φ is stoichiometrically related to electrons by a factor of 4 ($O_2 + 4e^- + 4H^+ \rightarrow 2H_2O$). R_{O_2} is 0.26 of Φ (Packard and Christensen, 2004), the factor tested in the arctic water column (Packard and Codispoti, 2007). R_{N_2} relates to ETS activity according to Codispoti and Packard (1980). Here, denitrifying waters occur between 93 and 233 m (shaded numbers). R_{CO_2} was calculated from both R_{O_2} and R_{N_2} (see Methods). Column 7 shows the modeled R_{CO_2} values below the R maximum (13m), obtained from the depth-normalized power function ($R_{CO_2} = R_m\ (z/z_m)^b$) fitted to the data in Column 6. The exponent, b, is always negative. F_C was determined by integrating either to the bottom (F_{t-s}, Column 8) or to infinity (F_∞, Column 9). The first represents the labile organic carbon consumed by R from the Ez (21m) to the bottom, while the second includes benthic R and carbon burial. The difference between F_∞ and F_{t-s} equals benthic R and the carbon burial rate (Column 10). Column 11 represents the carbon flux determined by trapezoidal approximation, which relates to F_{t-s} by the regression: F_{t-s} = 0.85 $F_{c_{trap}}$ - 0.54 (r^2=0.99, $p < 0.001$).

Depth z (m)	ETS Activity (neq min^{-1} L^{-1})	Φ (μmol O_2 h^{-1} m^{-3})	R_{O_2} (μmol O_2 h^{-1} m^{-3})	R_{N_2} (μmol N_2 h^{-1} m^{-3})	R_{CO_2} (μmol CO_2 h^{-1} m^{-3})	R_{CO_2} modeled (μmol CO_2 d^{-1} m^{-3})	F_C to bottom F_{t-s} (mmol C d^{-1} m^{-2})	F_C to infinity F_∞ (mmol C d^{-1} m^{-2})	Benthic respiration and burial F_∞ - F_{t-s}	C-Flux to bottom Trap Calc (mmol C d^{-1} m^{-2})
0.5	37.10	556.56	144.71	-	102.74	-	-	-	-	-
3	37.81	567.14	147.46	-	104.69	-	-	-	-	-
5	35.69	535.39	139.20	-	98.83	-	-	-	-	-
9	33.65	504.68	131.22	-	93.16	-	-	-	-	-
13	39.19	587.87	152.85	-	108.52	1629.67	-	-	-	-
21	15.34	230.16	59.84	-	42.49	707.39	19.71	20.07	0.36	25.49
31	8.79	131.81	34.27	-	24.33	359.18	14.68	15.04	0.36	20.16
93	0.44	-	-	0.25	0.44	53.09	6.31	6.67	0.36	7.38
233	0.35	-	-	0.20	0.35	10.74	3.02	3.38	0.36	3.38
465	0.05	0.75	0.19	-	0.14	3.23	1.66	2.03	0.36	1.76
698	0.01	0.14	0.04	-	0.03	1.59	1.14	1.50	0.36	1.20
930	0.02	0.23	0.06	-	0.04	0.97	0.85	1.21	0.36	0.90
1395	0.01	0.21	0.05	-	0.04	0.48	0.54	0.90	0.36	0.57
1860	0.01	0.13	0.04	-	0.02	0.29	0.36	0.73	0.36	0.40
4755	-	-	-	-	-	0.06	0	0.36	0.36	0

Table 3. R_{O_2} as μmol O_2 h^{-1} m^{-3} profiles in the microplankton along the C-line section in September 1976 (unshaded digits). In the OMZ depths (shaded values), $NO_3{}^-$ was the electron acceptor and N_2 was produced during denitrification (R_{N_2} as μmol N_2 h^{-1} m^{-3}). All the calculations here are based on ETS activity measurements; see details in section 2.3 and Table 2. C-Line position as well as JASON station number (parenthesis) are given. Depth (z) is in meters and *R* refers to either R_{O_2} or R_{N_2} depending on the shading.

C1 (22)		C3 (15)		C3 (21)		C5 (20)		C5 (37)		C8 (19)		C8 (36)		C10 (18)		C12 (17)		C12 (35)		C14 (16)	
z (m)	*R*	*z (m)*	*R*	*z (m)*	*R*	*z (m)*	*R*	*z (m)*	*R*	*z (m)*	*R*	*z (m)*	*R*	*z (m)*	*R*	*z (m)*	*R*	*z (m)*	*R*	*z (m)*	*R*
0.5	56.11	0.5	24.11	0.5	83.99	0.5	119.13	0.5	79.97	0.5	80.32	0.5	87.67	0.5	34.35	0.5	47.14	0.5	144.71	0.5	40.90
4	84.66	6	34.89	5	78.92	3	154.77	4	86.75	4	92.40	5	97.89	5	35.79	6	30.65	3	147.46	7	34.62
6	44.15	9	35.86	9	64.26	6	130.83	7	95.81	8	75.17	8	88.41	8	51.17	10	39.54	5	139.20	11	36.09
10	71.05	17	42.74	14	43.68	9	180.26	11	86.29	12	54.66	12	83.74	15	40.07	16	29.04	9	131.22	18	54.67
16	60.88	28	30.99	21	20.57	14	97.08	17	77.46	19	69.74	19	63.75	24	87.36	26	34.38	13	152.85	28	44.78
24	42.41	42	15.42	33	12.05	21	41.27	27	67.29	29	45.27	29	19.16	36	24.75	40	29.61	21	59.84	43	25.66
				47	3.15	93	0.48	40	71.55	93	1.12	44	18.08	233	0.16	233	0.09	31	34.27	100	4.51
				93	1.80	233	0.67			233	0.48	93	0.59	465	0.04			93	0.25	250	0.73
						465	0.09			465	0.62	233	0.15	1860	0.02			233	0.20	500	0.22
										930	0.36	465	0.04					465	0.19	750	0.11
										1395	0.22	698	0.03					698	0.04	1000	0.06
												930	0.05					930	0.06	2000	0.09
												1395	0.06					1395	0.05		
																		1860	0.04		

Table 4. Power functions for microplankton R (mmol CO_2 d^{-1} m^{-3}) as functions of normalized depth, R_{CO_2} = R_m $(z/z_m)^b$, where R_{CO_2} is the respiratory CO_2 production at any depth (z), R_m is the R maximum (mmol CO_2 d^{-1} m^{-3}) in the water column, z/z_m is the depth normalized by the depth at R_m, and b is the maximum curvature of the power function. Both z/z_m and b are unitless. Δ z represents the depth range of the R values considered. The table includes the r^2 from the least-square regression analysis of the R models (Sigma Plot ver 12.5) and the number of data considered (n). The significance level of the regressions is indicated by increasing numbers of stars. The last four columns represent the linear regression of the respiration-model verification analysis. The slope, the intercept and the r^2 are given. The n value for each verification analysis is the same as the n used for each R model (column 7). These R models are based on ETS activity data taken during R/V Eastward JASON-76 expedition, along the C-Line.

CUEA C-Line Position (JASON Station)	Δ z (m)	z_m (m)	R_m (mmol CO_2 d^{-1} m^{-3})	b	r^2	n	Modeled *vs* Calculated R_{CO_2} slope	intercept	r^2	n
C1 (22)	4-24	4	1.538	-0.355	0.864	4	0.975	25.24	0.878	4
C3 (15)	17-42	17	0.783	-1.109	0.929	3	1.041	20.42	0.926	3
C3 (21)	5-93	0.5	20.659	-1.080	0.972***	7	1.095	45.37	0.905**	7
C5 (20)	9-465	9	2.796	-1.655	0.951**	6	0.890	4.25	0.996**	6
C5 (37)	7-40	7	1.596	-0.192	0.873*	5	0.875	168.87	0.902*	5
C8 (19)	4-1395	4	3.247	-1.168	0.957***	10	1.348	129.78	0.686*	10
C8 (36)	5-1395	5	4.413	-1.670	0.949***	12	0.937	-44.14	0.808**	12
C10 (18)	24-1860	24	0.946	-2.051	0.962*	5	0.638	29.3	0.976*	5
C12 (17)	0.5-233	0.5	3.172	-0.720	0.497	7	2.596	-661.42	0.339	7
C12 (35)	13-1860	13	1.630	-1.740	0.948***	10	0.627	10.56	0.998**	10
C14 (16)	18-2000	18	1.183	-1.624	0.968***	9	1.043	-19.72	0.910**	9

*p<0.05
**p<0.001
***p<0.0001

Table 5. Microplankton respiration in epipelagic, mesopelagic, and bathypelagic waters along the C-Line across the Peru Current upwelling system at 15° S. Calculations are based on the R models in Table 4. Shoreward of C5 the bottom limits the lower depth boundary. Note the 1000-fold shift in the rates expressed per area (columns 3-7) and per volume (columns 8-10).

CUEA C-Line Position (JASON station)	Ocean depth (m)	Water column R (mmol C m^{-2} d^{-1})	Benthic respiration and C burial (mmol C m^{-2} d^{-1})	Epipelagic 1-150 m (mmol C m^{-2} d^{-1})	Mesopelagic 150-1000 m (mmol C m^{-2} d^{-1})	Bathypelagic 1000 m-bottom (mmol C m^{-2} d^{-1})	Epipelagic 1-150 m (μmol C m^{-3} d^{-1})	Mesopelagic 150-1000 m (μmol C m^{-3} d^{-1})	Bathypelagic 1000 m-bottom (μmol C m^{-3} d^{-1})
C1 (22)	63	53.98	-	53.98	-	-	856.85	-	-
C3 (15)	117	80.32	99.23	80.32	-	-	686.50	-	-
C3 (21)	120	45.81	82.99	45.81	-	-	381.75	-	-
C5 (20)	550	252.48	2.60	248.99	3.49	-	1659.96	8.72	-
C5 (37)	607	507.91	-	162.98	344.93	-	1086.51	754.78	-
C8 (19)	1880	82.10	27.37	67.58	11.46	3.07	450.51	13.48	3.49
C8 (36)	2150	153.46	0.57	150.65	2.43	0.38	1004.36	2.85	0.33
C10 (18)	4300	1256.23	0.09	1262.18	2.72	0.34	8414.54	3.20	0.10
C12 (17)	4000	64.36	-	22.28	19.57	22.51	148.55	23.02	7.50
C12 (35)	4755	318.83	0.36	314.51	3.53	0.79	2096.75	4.16	0.21
C14 (16)	2680	318.14	1.50	310.56	6.30	1.28	2070.43	7.41	0.76

Table 6. Carbon flux models F_C at C-Line positions deeper than 500 m in the Peru Upwelling System September 1976. From these models, F_C at four different depths were determined. NRE and F_C Transfer Efficiency (T_{eff}) for the upper mesopelagic waters (150-500m) are also given. NRE was calculated as 100 x $R_{CO_2}/F_{c_{150}}$, where the R_{CO_2} represents the integrated R between 150-500m; T_{eff} was calculated as 100 x $F_{c_{500}}/F_{c_{150}}$ according to Buesseler et al. (2007).

CUEA C-Line Position (JASON Station)	Ocean depth (m)	Euphotic zone, z_e (m)	F_C models	F_C from z_e (mmol C m^{-2} d^{-1})	F_C from 150 m (mmol C m^{-2} d^{-1})	F_C from 500 m (mmol C m^{-2} d^{-1})	F_C from 1000 m (mmol C m^{-2} d^{-1})	NRE 150-500 m (%)	T_{eff} 150-500 m (%)
C5 (20)	550	21	$22.07(z/z_e)^{-0.655}$	22.07	6.09	2.77	-	54.6	45.4
C8 (19)	1880	29	$55.25(z/z_e)^{-0.168}$	55.25	41.92	34.24	30.48	18.3	81.7
C8 (36)	2150	29	$10.14(z/z_e)^{-0.670}$	10.14	3.37	1.51	0.95	55.4	44.6
C10 (18)	4300	36	$14.11(z/z_e)^{-1.051}$	14.11	3.15	0.89	0.43	71.8	28.2
C12 (35)	4755	21	$20.07(z/z_e)^{-0.740}$	20.07	4.68	1.92	1.15	59.0	41.0
C14 (16)	2680	43	$19.80(z/z_e)^{-0.624}$	19.80	5.81	2.74	1.78	52.8	47.2

Table 7. HEP as ATP production in epipelagic, mesopelagic, and bathypelagic waters of the C-Line section, September 1976. Shoreward of C5 the bottom limits the lower depth boundary.

CUEA C-Line Location (JASON station)	Ocean depth (m)	Epipelagic HEP 1-150 m (J m^{-3} d^{-1})	Mesopelagic HEP 150-1000 m (J m^{-3} d^{-1})	Bathypelagic HEP 1000 m-bottom (J m^{-3} d^{-1})
C1 (22)	63	289.63	-	-
C3 (15)	117	232.05	-	-
C3 (21)	120	173.40	-	-
C5 (20)	550	977.93	1.19	-
C5 (37)	607	367.24	255.11	-
C8 (19)	1880	138.77	3.59	0.89
C8 (36)	2150	319.41	0.80	0.09
C10 (18)	4300	2609.16	0.89	0.03
C12 (17)	4000	43.60	4.56	1.23
C12 (35)	4755	535.98	1.18	0.06
C14 (16)	2680	699.88	2.51	0.26